NEAR-WALL TURBULENCE IN JET IMPINGEMENT ON A WALL

G. F. Gorshkov

UDC 532.526

In subsonic axisymmetric jet impingement on a plane wall perpendicular to the jet axis, it is possible to identify a number of characteristic flow regions within the initial (Fig. 1a) or the basic (Fig. 1b) flow regions: the undisturbed jet flow region I covering the distance from the nozzle exit to the wall $H = h/r_a \geq 3$, where r_a is the radius of the nozzle section; the mixing region II, where the flow turns along the wall with appreciable negative pressure gradient along the wall; the radial wall jet region III and the near-wall boundary-layer region IV.

Gas flow in these regions is characterized by nonuniform distribution in mean and fluctuating characteristics along longitudinal and transverse directions [1] and high level of fluctuations in gasdynamic quantities (flow turbulence) affecting heat-and-mass transfer in the near-wall boundary layer [2, 3]. The nature of gas flow in the boundary layer near the stagnation point is such that, in setting up the turbulence model for the closure of basic equations, it is not possible to correctly simulate the actual momentum, heat, and mass transfer within the framework of simplest phenomenological first-order derivative models (e.g., Prandtl's mixing length model) because of a number of reasons. Unfortunately, there is very little information on the microstructure of axisymmetric flow in the above-mentioned flow regions in jet impingement on a plane wall. Apart from [1-4], it is possible to mention [5], in which plane jet impingement is considered. The aim of the present paper is to consolidate and generalize the available data on the microstructure of axisymmetric jet impingement.

1. Experimental Procedure and Data Processing. The study was conducted on an experimental setup [1, 4] using constant temperature hot-wire anemometer (frequency domain for the instrument was up to 25 kHz) with the following range of parameters: nozzle diameter d_a = 30-100 mm with a contraction ratio (by area) of 100-9, respectively; mean exit velocity $\langle U_a \rangle$ = 8-100 m/sec; distance to the obstacle H = 1-32; Reynolds number $Re_a = \langle U_a \rangle d_a/\nu = 10^4$-$10^5$, initial turbulence at the nozzle center ε_a = 1.5%. Large contraction ratio Vitoshinskii nozzle ensured uniform mean velocity profile and its fluctuations at the nozzle section. The state of the boundary layers at the nozzle exit section (only they determine the initial nonuniformity in parameters) was estimated directly from mean velocity and turbulence measurements as well as from extensive experimental data given in [6-8]. The flow condition in the boundary layer depends on many factors, first of all on Re_a and nozzle contraction ratio. For example, when $\langle U_a \rangle$ = 8 m/sec for 30- and 100-mm diameters, the initial boundary layer is characterized by the following parameters: d_a = 30 mm results in laminar boundary layer with shape factor $H_\delta = \delta^*/\delta^{**} \approx 2.5$, with momentum thickness $\delta^{**}/r_a = 0.025$ and maximum fluctua-

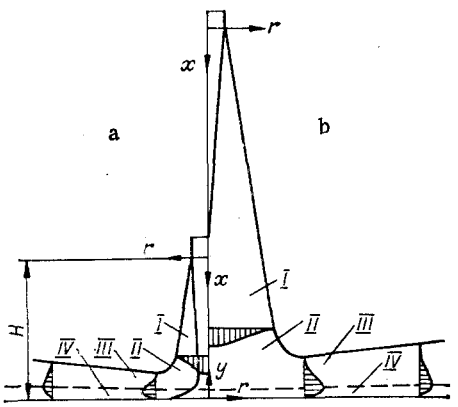

Fig. 1

Leningrad. Translated from Zhurnal Prikladnoi Mekhaniki i Tekhnicheskoi Fiziki, No. 2, pp. 73-82, March-April, 1984. Original article submitted January 4, 1984.

0021-8944/84/2502-0233$08.50

tion level $\varepsilon_{a\max} \approx 5\%$; when $d_a = 100$ mm, there is a turbulent boundary layer with $H_\delta \approx 1.46$, $\delta^{**}/r_a \approx 0.014$, and $\varepsilon_{a\max} \approx 12\%$.

The following were studied: streamwise R_{1x} and transverse R_{1r} correlation coefficients

$$R_{1x,r} = \langle u'(0)u'(\Delta x,\ \Delta r)\rangle/(\langle u'^2(0)\rangle\langle u'^2(\Delta x,\ \Delta r)\rangle)^{1/2},$$

where <u'(0)u'(Δx)> and <u'(0)u'(Δr)> are, respectively, the streamwise and transverse spatial correlation between fluctuations u' in the axial velocity component at two different points in the flow (only the behavior of the axial component of velocity fluctuation is considered here and in what follows); angular brackets denote time-averaged quantity; integral scale of turbulence in the streamwise and transverse directions is

$$L_{1x,r} = \int_0^\infty R_{1x,r}dx, r;$$

normalized energy spectrum (frequency of turbulence energy distribution), $-F_1(n) = E_1(n)/\langle U\rangle$, where $E_1(n)$ is the distribution function for velocity fluctuation, n is the frequency, for which

$$\int_0^\infty F_1(n)\,dn = 1.$$

The measurement of streamwise and transverse correlation coefficients was made with two single-element transducers, one of them being stationary and the other was moved downstream for measuring R_{1x} and along the normal to the basic flow direction for measuring R_{1r}. Analog correlator with a 10 Hz–20 kHz bandpass filter was used to determine $R_{1x,r}$. While measuring R_{1x} as $\Delta x \to 0$, the element located downstream is influenced by the aerodynamic wake of the first element and hence the value of the correlation coefficient happens to be lower. In order to avoid this problem, in accordance with recommendations of [9], the second element was laterally moved by 0.2 mm or even rotated through 90° relative to the first element. The transverse correlation coefficients in the near-wall boundary layer were determined in two ways: The transducer 2 (Fig. 2b) was located at a known distance from the wall y_2 and the transducer 1, closest to the wall, was moved downstream toward the wall relative to the first; the transducer 1 was kept at a minimum distance from the wall ($y_1 = 0.1$ mm) and the transducer 2 was moved up relative to the first from the wall. The measurement of streamwise correlation coefficient in the boundary layer was not carried out due to large errors in measurements arising from aerodynamic wake behind the probe and its support.

The quantities L_{1x} and L_{1r} were determined by computing the areas under the curves R_{1x} and R_{1r}. The area bounded by the first intersection of the curve with abscissa was taken into account.

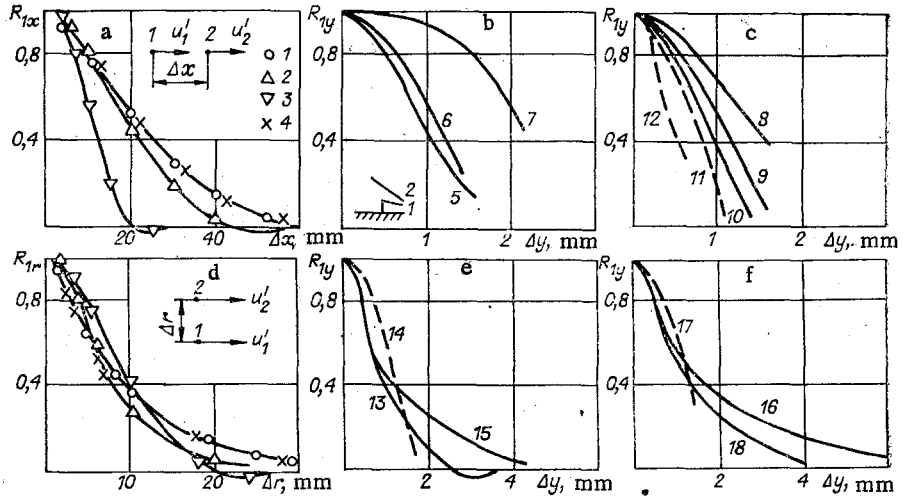

Fig. 2

The spectra of streamwise velocity fluctuations were studied with a spectrum analyzer and frequency characteristics. The total permissible frequency range was 20-20,000 Hz. In the analysis of spectral function, the probe diameter was 5 μm and the signal-to-noise ratio was 10^{-6}-10^{-7}.

Since turbulence can be considered a stationary random process, there is a connection between correlation and spectral functions expressed by Fourier integral transform [10]:

$$R_{1x} = \int_0^\infty F_1(n) \cos \frac{2\pi n x}{\langle U \rangle} dn; \tag{1.1}$$

$$F_1(n) = \frac{4}{\langle U \rangle} \int_0^\infty R_{1x} \cos \frac{2\pi n x}{\langle U \rangle} dx. \tag{1.2}$$

For isotropic turbulence as $n \to 0$, Eq. (1.2) reduces to the known ratio for integral scale in the axial direction

$$L_{1x} = F_1(0)\langle U \rangle/4, \tag{1.3}$$

where $F_1(0)$ is the value of the spectral density as $n \to 0$. It is necessary to mention that though Eq. (1.2) permits the determination of $F_1(n)$ by analytical approximation of R_{1x}, the existing experimental spectral as well as correlation function methods still lead to large errors. Hence the relation between spectral and correlation functions should be considered mainly to verify the results of the experimental determination of each one of them.

2. Results of Investigation. Free Hot Jet (Undisturbed Flow Region). Experimental results for streamwise and transverse correlation coefficients in free jet (Fig. 2a, c, curves 4, with x = 6 and r = 0 for d_a = 100 mm and $\langle U_a \rangle$ = 8 m/sec; here and in what follows all linear dimensions, as well as integral scales, are referred to nozzle section diameter r_a) confirmed the known behavior of correlation curves. Thus, correlation coefficient $R_{1x,r}$ changes with the range $R_{1x,r} \in [0; 1]$ where the reduction in $R_{1x,r}$ with increase in Δx and Δr can be monotonic as well as fluctuating. It is necessary to mention that the nature of variation of R_{1x} and R_{1r} is identical through the extent of dependence of streamwise correlation and is considerably more than the transverse.

The distribution of integral turbulent scales L_{1x} and L_{1r} (Fig. 3a, d_a = 30-100 mm; $\langle U_a \rangle$ = 8-100 m/sec; bright signs represent L_{1x}, dark signs are for L_{1r}, positions 1, 3, and 7 are the data on the line r = 1; 2, 4, and 8 for r = 0; 9 is from experiment [11]; 10 from [12]), computed from correlation curves R_{1x} and R_{1r} across mixing zone showed that the maximum values of integral scales occur inside the mixing zone of the jet at x ≈ 20. However, the linear variation of axial integral scale with distance (curve 5), suggested in [12],

$$L_{1x} = 0.13x$$

is true only in the immediate neighborhood of nozzle section ($x \in [0; 3]$). With further streamwise turbulence the integral scale along the lines r = 1 and 0 can be described by the following approximate relations (curves 1 and 2, respectively):

$$L_{1x} = 0{,}13x^{0{,}89} \exp(-0{,}048x), \quad L_{1xm} = 0{,}13x^{0{,}92} \exp(-0{,}043x)$$

for $x \in [0; 40]$ where the index m corresponds to the parameters on the jet axis.

The variation in transverse turbulence integral scale is practically linear with increase in x within the limits $x \in [0; 16]$ and is also described by empirical relations obtained along lines r = 1 and 0 (curves 3 and 4, respectively):

$$L_{1r} = 0{,}036x + 0{,}026, \quad L_{1rm} = 0{,}026x + 0{,}056.$$

Investigation of Mach and Reynolds numbers in the above range of M_a and Re_a showed their very weak influence on L_{1x} and L_{1r} in the entire expansion region of the jet.

Analysis of the results of measurements of correlations of experimental curves given in the present paper and [11] made it possible to obtain the following relations coupling correlation coefficients R_{1x} and R_{1r} with nondimensional length $\Delta x/L_{1x}$ and $\Delta r/L_{1r}$:

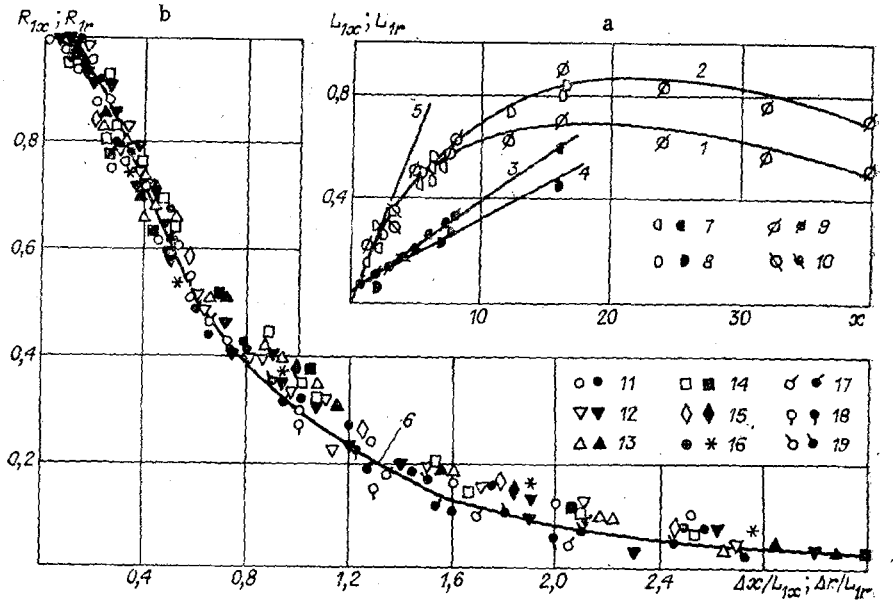

Fig. 3

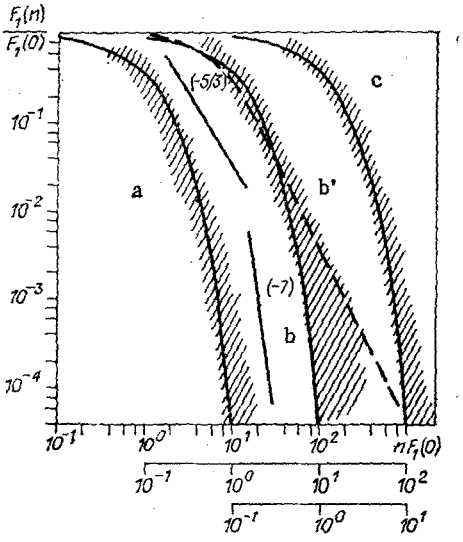

Fig. 4

$$R_{1x} = \left[1 + \frac{\pi^2}{4}\left(\frac{\Delta x}{L_{1x}}\right)^2\right]^{-1}; \tag{2.1}$$

$$R_{1r} = \left[1 + \frac{\pi^2}{4}\left(\frac{\Delta r}{L_{1r}}\right)^2\right]^{-1}. \tag{2.2}$$

Computed results (curve 6) from (2.1) and (2.2) are given in Fig. 3b, where bright signs denote R_{1X} and dark ones indicate R_{1r}; positions 11, 12...16 are from the present experiment for the jet coordinates: 11) x = 2, r = 0; 12) 2, 1; 13) 6, 1; 14) 6, 0; 15) 16, 0; 16) 16, 1; positions 17, 18, and 19 are from the experiment [11].

Spectral analysis of axial component of velocity fluctuations showed that for a fixed velocity at the nozzle section the contribution from low-frequency fluctuations increases with the distance from the axis of the jet and the contribution from high-frequency fluctuations decreases; with increase in velocity at the nozzle section the spectrum is shifted toward the higher frequency region; with increase in the distance from the nozzle section the spectrum is shifted to the low-frequency region.

The generalized curve for spectral density $F_1(n)/F_1(0)$ is shown in Fig. 4a for hot subsonic jet as a function of $nF_1(0)$ at different values of critical parameters; here the shaded region (experiment) corresponds to the following flow parameters: $\langle U_\alpha \rangle$ = 8, 18.5 m/sec, d_α = 30, 100 mm, x = 0-14, r = 0-1.66.

It follows from an analysis of the data that the normalized spectral density in terms of frequency in the entire jet is self-similar in nature and could be described by the relation (curve a) obtained on the basis of Fourier integral transform (1.2) by substituting correlation function R_{1x} (2.1) in it:

$$\frac{F_1(n)}{F_1(0)} = \left[1 + \frac{\pi^2}{4} n^2 F_1^2(0)\right]^{-1}. \tag{2.3}$$

An attempt to construct spectral density in the coordinates of wave number $k_1 = 2\pi n/\langle U \rangle$, m^{-1}, did not provide a positive result. This is obviously because the wave number $k_1 \sim L^{-1}{}_{1x}$ in the jet flow is appreciably nonconstant (depends on coordinates x and r). If Eq. (1.3) is used, then it is possible to show that $nF_1(0) = 2/\pi k_1 L_{1x}$ and the complex $nF_1(0)$ is more universal since the integral scale is included in it. Similar expression of spectral density [$k_1F_1(k_1) = f(k_1L_{1x})$] for plane channel flow is given in [9], where it is shown that in this case a universal distribution is observed in the low-wave number region, i.e., for large-scale turbulence, whereas for large-scale wave numbers there is a divergence of spectral density curves obtained at different points in the channel.

The spectral density distributions obtained here were compared with the known Kolmogorov law for the universality of microscale turbulent fluctuations [$E_1(k_1) \sim k_1^{-5/3}$]. As seen from Fig. 4, the inertial flow region is small. In the region of large wave numbers, results of the present work satisfactorily represent angular coefficient (—7).

3. Mixing Region. The variation of streamwise and transverse correlation coefficients along the axis of the mixing region of the jet with the wall is shown in Fig. 2a, c as a function of the distance y for $\langle U_\alpha \rangle$ = 8 m/sec, d_α = 100 mm, H = 8, r = 0. Experimental data correspond to the following distances y from the surface of the wall: 1) y = 2; 2) y = 1; 3) y = 0.5. It must be remembered that here the curves R_{1x} and R_{1r} are plotted on the free jet axis for x = 6 (curve 4).

Analysis of experimental data for the coefficient R_{1x} in the free (curve 4) and mixing regions of the jets (curves 1-3) makes it possible to conclude that the wall has appreciable influence on the behavior of the streamwise correlation coefficient: The variation in R_{1x} with a decrease in y (y < 2) becomes steeper. As regards the variation in coefficients R_{1r}, the wall has less effect on them compared to R_{1x} for the given range of parameters. The above-mentioned nature of the behavior of R_{1x} with decrease in y is also confirmed by the experiment [5] for the case of a plane jet mixing region when h/b = 100, where b is the nozzle width.

The curves for the distribution of correlation coefficients were integrated in order to obtain integral scales in the mixing region. It follows from data analysis that if, in the free hot jet, the value of axial integral scale increases along the axis with coordinate x, attaining its maximum value at x ≈ 20 (see Fig. 3a), then in the mixing zone L_{1x} decreases to zero as the wall is approached. When y = 2, the value of L_{1x} corresponds to the value of L_{1x} in the free jet.

Distribution of integral scale L_{1r} in the mixing zone is subject to the distribution laws of L_{1r} in the free jet and the numerical values of integral scales are determined by the distance of the nozzle section from the wall H.

Analysis of experimental results on integral turbulence scales L_{1x} and data [5] in the mixing region on the jet axis made it possible to obtain the following approximate relation to determine L_{1x} in the form [13]:

$$L_{1x}/H = 0.81\zeta - 3.85\zeta^2 + 6.37\zeta^3,$$

where

$$\zeta = y/H \text{ for } H \in [3;\ 17],\ \zeta \in [0;\ 0.25].$$

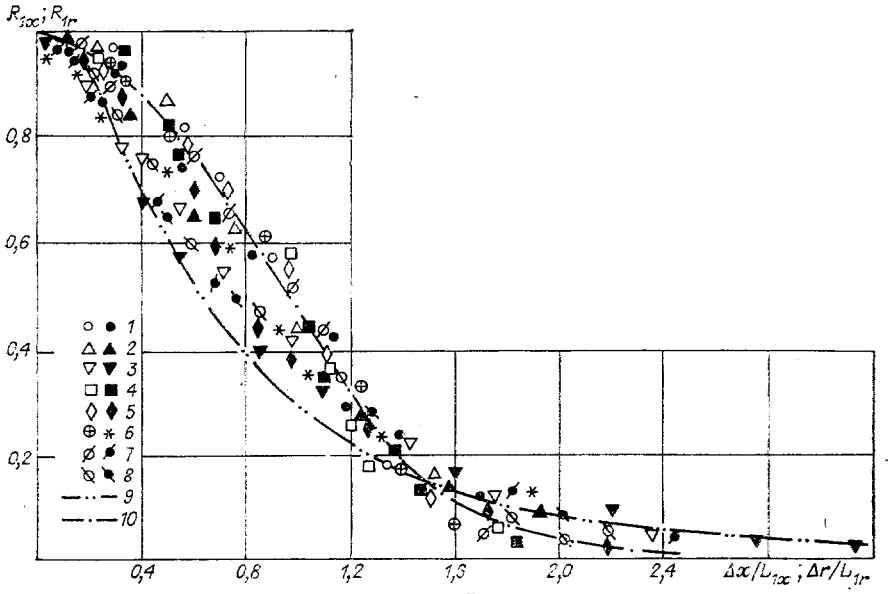

Fig. 5

These values of integral scales L_{1x} and L_{1r} were used both in the case of the flow in the free jet to analyze the distribution of correlation coefficients R_{1x} and R_{1r} as well as $f(\Delta x/L_{1x})$ and $f(\Delta r/L_{1r})$. Data from the above analysis are given in Fig. 5. Light signs denote R_{1x} and the dark signs represent R_{1r} for the following set of parameters: 1) H = 8, d_a = 100 mm, y = 0.5; 2) 8, 100, 1; 3) 8, 100, 2; 4) 8, 40, 0.5; 5) 8, 40, 1; 6) 17, 40, 1; 7) 17, 40, 0.5; 8) 17, 40, 2. Equations (2.1) and (2.2) (curve 9) and relations from [10] (curve 10) are also shown here in the form

$$R_{1x} = \exp\left(-\frac{\pi}{4}\frac{\Delta x^2}{L_{1x}^2}\right); \tag{3.1}$$

$$R_{1r} = \exp\left(-\frac{\pi}{4}\frac{\Delta r^2}{L_{1r}^2}\right). \tag{3.2}$$

Analysis of experimental data shows that with the approach of the wall for $y \in [0; 1[$ correlation curves are fuller and follow Eqs. (3.1) and (3.2). With increasing distance from the wall for y > 1, correlation functions are less full and correspond to Eqs. (2.1) and (2.2). Thus, distributions R_{1x} and R_{1r} are not universal in the mixing region, although they could be obtained from (2.1), (2.2), and (3.1), (3.2) as a function of y.

The changes in the behavior of correlation curves lead to a change in the one-dimensional spectrum. The velocity at the nozzle section, as before, has the same effect on the nature of the spectrum as in the free jet. With approaching wall, as $\langle U_a \rangle$ = const, there is an increase in the contribution from low-frequency fluctuations as a result of stagnation at the wall.

The distribution of $F_1(n)$ in the mixing zone is shown in Fig. 4b. The dashed line corresponds to $\langle U_a \rangle$ = 8, 16 m/sec, d_a = 100 mm, H = 8 and 16, y = 0.2-2, r = 0-2.8.

It follows from the graph that in the high-frequency region the spectral distribution function is not universal in nature: experimental values of $F_1(n)/F_1(0)$ are placed between Eq. (2.3) (curve b) and the relation obtained from Eq. (3.1) using Fourier integral transform (1.2) (curve b'), in the form

$$F_1(n)/F_1(0) = \exp\,[-nF_1(0)]. \tag{3.3}$$

4. Near-Wall Boundary Layer. Some experimental results for transverse correlation coefficients R_{1y} in the near-wall boundary layer are shown in Fig. 2b, c, e, and f. It follows from the experimental data that, for y_2 = 1.7 mm and r = 1.6 = const (Fig. 2b, curves 5-7 correspond to H = 1, 8, and 16 for d_a = 100 mm) with an increase in the distance of the nozzle section from the wall H there is an increase in the fullness of profiles R_{1y}. On the other hand, for H = 1 = const and y_2 = 1.7 mm (Fig. 2c, curves 8-10 correspond to r = 0.8,

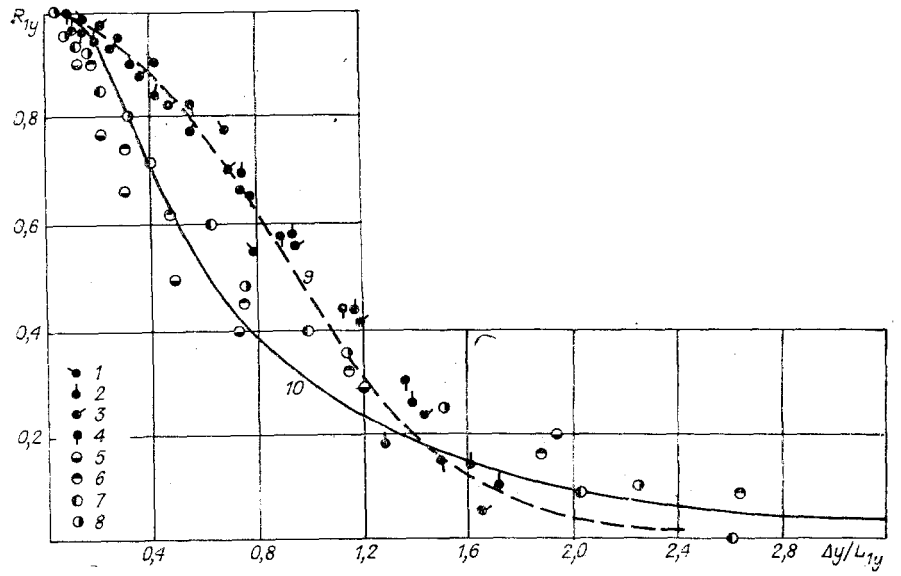

Fig. 6

TABLE 1

d_a, mm / H	r / y, mm →	0,1	0,85	1,0	1,2	1,7	2,3	L_{1y}
100/1	0,8 1,6 2,4				0,974 0,73 0,83	1,2 0,95		0,0217 0,0168 0,0167
100/8	1,6 2,4					1,03 0,85		0,0206 0,0170
100/16	0,8 1,6 2,4 3,0	 2,20	0,83 0,65 0,66				2,0 1,98 1,77 1,72	0,0283 0,0396 0,0242 0,0305
30/30	1,6 6,0 10,0	 1,33		0,79 0,74 0,75		1,24 1,09 1,19		0,0675 0,0607 0,0727

TABLE 2

d_a, mm / H	r / y, mm →	0,1	0,2	0,3	0,4	1,0	1,8	L_{1r}
100/1	1,6	4,65		5,0		17		0,338
100/4	0,8 1,6				5,2 12,1	1,4 14,6		0,148 0,292
100/8	0,8 1,6 2,4		2,38	7,2		9,5 17,2 19,2		0,190 0,347 0,384
30/16	0,8 1,6 2,67 10,0	2,63 2,19 2,0				4,7 9,05 12,4 6,5	 6,0	0,313 0,603 0,827 0,430
30/30	2,67 6,0 8,0 10,0		2,95 3,12 2,74 2,52		6,26	9,65 10,2 9,05 8,35	 11 10	0,643 0,680 0,630 0,556

1.6, and 2.4 for d_a = 100 mm) with increase in the distance from the stagnation point r there is a reduction in the fullness of the profile R_{1y}. It is necessary to mention that the greater is the damping of correlation curves R_{1y} the lower is the distance y_2 from the wall (curves 9, 11, and 12 are for y_2 = 1.7, 1.2, and 0.7 mm for d_a = 100 mm) with H and r = const. From a comparison of distribution curves for R_{1y}, viz., 13, 14 or 16, 17 (Fig. 2e, curves 13 and 14 correspond to y_1 = 0.1 mm, y_2 = 1.6 for d_a = 30 mm, H = 16, and r = 5.5; Fig. 2f, curves 16 and 17 are for y_1 = 0.1 mm and y_2 = 1.6 for d_a = 30 mm, H = 30, and r = 5.5), it follows that the nature of variation of R_{1y} depends on the distance from the first measurement point over the wall surface (displacement of the moveable transducer away from the wall or toward it). Thus, as the transducer moves away from the wall (y_1 = 0.1 mm, curves 13, 15, and 16, 18; positions 15 and 18 correspond to r = 10) the extent of the region continuous in Δy is 2-3 times higher than during the motion toward the wall (curves 14 and 17) and significantly exceeds the wall boundary-layer thickness, which indicates the deep penetration of large-scale vortices from the jet to the wall boundary layer and the asymmetry in correlation function relative to the origin.

Integral scales L_{1y} were determined from the distribution of R_{1y}. The streamwise integral turbulence scale L_{1r} is plotted using Eq. (1.3). Numerical values of L_{1y} and L_{1r} (in millimeters) are given in Tables 1 and 2. The arithmetic mean value of the scale L_{1y} for all y across the boundary layer is also given in Table 1 in the last column. It is conditionally taken as the integral scale at the outer boundary of the boundary layer. In Table 2 the values of L_{1r} at the boundary-layer edge (the last column) correspond to the distance y = 1 mm. Analysis of these data shows that within the framework of the present study the quantity L_{1y} can be considered a constant, being of the order of the boundary-layer thickness. The quantity L_{1r} considerably exceeds L_{1y}, and it increases with an increase in the distance from the stagnation point r, attaining a certain maximum at r $\simeq$ 4 and then decreases. With increase in y from the wall as r and H = const, the streamwise integral turbulence scale increases (see Table 2).

Analysis of correlation functions R_{1y} in the $\Delta y/L_{1y}$ coordinates (Fig. 6, where the dark points denote the movement of the transducer 1 downstream toward the wall with y_2 = 1.7 mm = const; the light points correspond to movement of the transducer 2 upward from the wall with y_1 = 0.1 mm = const for the following set of parameters: 1) H = 1, r = 1.6; 2) 1, 6; 3) 8, 2.4; 4) 16, 6; 5) 16, 3; 6) 16, 10; 7) 16, 5.3; 8) 30, 10) showed that the behavior of correlation functions as the transducer moves toward the wall can be described by Eq. (3.2), i.e., curve 9, and by Eq. (2.2) as the transducer moves away from the wall (curve 10). The above situation may be associated with the influence of the wall on the jet in the mixing region and also with the inaccuracy in the determination of correlation coefficients.

It follows from the analysis of energy spectra for the above range of flow parameters that the maximum frequency varies from 1 kHz at the outer boundary with velocity at the nozzle exit $\langle U_a \rangle$ = 8 m/sec to 0.5 kHz for y = 0.1 mm. The upper value of the frequency in free jet and in the mixing region equals 2 kHz. The expression of the one-dimensional spectrum of streamwise velocity fluctuations in the form (2.3) (see Fig. 4c, curve c) carries a self-similar characteristic in the wall region of the boundary layer (dashed region corresponds to the following interaction parameters: d_a = 30 and 100 mm, H = 1-16, r = 0.8-6, y = 0.1-1.4 mm). The presence of spectral self-similar function (2.3) makes it possible to describe the distribution of streamwise correlation coefficient R_{1r} in the boundary layer using Fourier integral transform also by the universal relation (2.1).

In conclusion, it is necessary to mention the equations (2.1)-(2.3) and (3.1)-(3.3) characterizing, as a rule, isotropic turbulence, are also valid (within experimental errors) for real nonisotropic flow, which makes it possible to consider the microstructure of the flow to be locally isotropic and the relations themselves to be an interesting approximation for practical computations of jet impingement on a wall.

LITERATURE CITED

1. I. A. Belov, G. F. Gorshkov, et al., "Experimental study of gasdynamic parameters in jet impingement on a wall," Izv. Akad. Nauk SSSR, Mekh. Zhidk. Gaza, No. 2 (1971).
2. G. F. Gorshkov, I. A. Belov, and V. S. Terpigorev, "Heat-transfer processes and boundary-layer microstructures near the stagnation point of jet impingement on a wall," in: Heat and Mass Transfer, VI [in Russian], Vol. 1, Part 2, Institute of Heat and Mass Transfer, Academy of Sciences of the Belorussian SSR, Minsk (1980).

3. E. P. Dyban and É. Ya. Épik, "Influence of free-stream turbulence on heat transfer in turbulized boundary-layer flows," in: Heat and Mass Transfer - VI [in Russian], Vol. 1, Part 2, Institute of Heat and Mass Transfer, Academy of Sciences of the Belorussian SSR, Minsk (1980).
4. I. A. Belov, G. F. Gorshkov, et al., "Effect of jet turbulence on the near-wall boundary-layer flow," Prikl. Mekh. Tekh. Fiz., No. 6 (1972).
5. E. Gutmark, M. Wolfshtein, and I. Wygnanski, "The plane turbulent impinging jet," J. Fluid Mekh., 88, 4 (1978).
6. A. N. Sekundov and O. V. Yakovlevskii, "Some problems in transition of channel flow into a jet," Izv. Akad. Nauk SSSR, Mekh. Zhidk. Gaza, No. 3 (1967).
7. A. K. M. F. Hussain and M. F. Zedan, "Effects of the initial condition on the axisymmetric free shear layer: effects of the initial momentum thickness," Phys. Fluids, 21, No. 7 (1978).
8. A. K. M. F. Hussain and M. F. Zedan, "Effects of the initial condition on the axisymmetric free shear layer; effect of the initial fluctuation level," Phys. Fluids, 21, No. 9 (1978).
9. J. Cont-Bello, Turbulent Flow in Channel with Parallel Walls [Russian translation], Mir, Moscow (1968).
10. J. O. Hinze, Turbulence. An Introduction to Its Mechanism and Theory, McGraw-Hill, New York (1959).
11. J. C. Lawrence, "Intensity, scale, and spectra of turbulence in mixing region of free subsonic jet," NASA Rep. 1956, No. 1292.
12. P. O. A. L. Devies and M. G. Fisher, "The characteristics of the turbulence in the mixing region of a round jet," J. Fluid Mech., 15 (1963).
13. G. F. Gorshkov, "Microstructure of the flow in the mixing region," in: Proceedings of All-Union Scientific Conference on Jet Flows, Novopolotsk Polytechnical Institute Press, Novopolotsk (1982).

NONLINEAR FORCED VIBRATIONS IN A HELMHOLTZ RESONATOR

N. A. Borisova, A. P. Golovin, A. V. Gubarev, S. A. Laptev, A. A. Nekrasov, and O. I. Pechenova

UDC 533.534-13

The linear theory of a Helmholtz resonator — a vessel with a short open neck — was developed by Helmholtz and Rayleigh. In this theory [1], a Helmholtz resonator is treated as a vibrating system with one degree of freedom (for the fundamental longitudinal mode), and in the first approximation it is assumed that all its kinetic energy is concentrated in the moving gas in the neck and in a certain neighborhood of the neck opening, and the potential energy of elastic deformation is in the gas in the vessel. The Helmholtz resonator is distinguished by its high Q, which is responsible for its wide use in acoustics. The process characterized by a periodic directed ejection of gas from a Helmholtz resonator with a subsequent suction of a new portion of gas from the space surrounding the neck inlet determined its technical use in devices providing pulsed periodic combustion of fuel [2, 3]. The Helmholtz resonator can clearly be used in other devices also, in which pulsed periodic physical and chemical reactions and technological processes occur with the release of energy in gas mixtures, for example in a pulsed periodic gas laser. For a technical device it is important to intensify the process; in a Helmholtz resonator this involves the excitation of strong intrinsically nonlinear vibrations [2, 3] in which the flow velocity in the neck turns out to be comparable with the velocity of sound. For such devices it is necessary to know the variation in the flow rate and the intensity of mass transfer in the neck, which also determines their efficiency. It is clear that such information can be obtained for nonlinear vibrations only by numerical methods.

Moscow. Translated from Zhurnal Prikladnoi Mekhaniki i Tekhnicheskoi Fiziki, No. 2, pp. 82-87, March-April, 1984. Original article submitted January 3, 1983.

0021-8944/84/2502-0241$08.50